Supplementary Online Materials

For

Magneto-impedance spectroscopy of epitaxial multiferroic thin films

Rainer Schmidt[1,*], Jofre Ventura[2], Eric Langenberg[2,3], Norbert M. Nemes[1], Carmen Munuera[4], Manuel Varela[2], Mar Garcia-Hernandez[4], Carlos Leon[1], Jacobo Santamaria[1]

[1] *Universidad Complutense de Madrid, GFMC, Dpto. Física Aplicada III, Facultad de Ciencias Físicas, 28040 Madrid, Spain*

[2] *Universitat de Barcelona, Dpto. Física Aplicada i Óptica, Diagonal Sud, Facultats de Física i Química, Martí i Franquès 1, 08028 Barcelona, Spain*

[3] *Universidad de Zaragoza, Instituto de Nanociencia de Aragón, Mariano Esquillor, 50018 Zaragoza, Spain*

[4] *Instituto de Ciencia de Materiales de Madrid - Consejo Superior de Investigaciones Científicas (ICMM-CSIC), Sor Juana Inés de la Cruz 3, 28049 Madrid, Spain*

*Corresponding author. Electronic mail: rainerxschmidt@googlemail.com

I. Dielectric spectroscopy

Temperature dependent impedance spectroscopy (IS) enables different contributions to the dielectric and resistive properties of condensed matter to be deconvoluted and characterized separately. IS is therefore the method of choice to separately determine and investigate the dielectric properties of intrinsic film and extrinsic Maxwell-Wagner type interface contributions in electrically inhomogeneous BMO and BFO thin film structures. IS experiments consist of a time (t)-dependent alternating voltage signal U of angular frequency ω ($\omega = 2\pi f$) and amplitude U_0 applied to the sample, and effectively the phase shift δ and amplitude I_0 of the current response signal I are measured.[1,2]

$$U(\omega, t) = U_0 \cos(\omega t); \qquad \text{(SOM 1)}$$

$$I(\omega, t) = I_0 \cos(\omega t - \delta); \qquad \text{(SOM 2)}$$

Parameters defined by the applied voltage signal are printed in blue, the measured parameters of the current response are in red. The current response of ideal circuit elements is: (1) in-phase with the applied voltage in the case of an ideal resistor R ($\delta = 0$); (2) out-of-phase by $\delta = -\pi/2$ for an ideal capacitor C; and (3) out-of-phase by $\delta = +\pi/2$ for an ideal inductor. All phase angles are time independent for a given frequency which allows the impedance to be defined as a time-independent complex number Z^* ($= Z' + iZ''$). From the phase angle δ and the current amplitude I_0, the impedance modulus $|Z|$, the real and imaginary parts of the impedance Z' and Z'', dielectric permittivity ε' and ε'', and conductivity σ' and σ'' can be determined:

$$|Z| = \frac{U_0}{I_0};\ Z' = |Z|\cos\delta\ ;\ Z'' = |Z|\sin\delta; \qquad \text{(SOM 3)}$$

$$\varepsilon' = \frac{-Z''}{\omega\varepsilon_0 g\ \left(Z'^2 + Z''^2\right)} = \frac{-\sin\delta}{\omega\varepsilon_0 g\ |Z|};\ \varepsilon'' = \frac{Z'}{\omega\varepsilon_0 g\ \left(Z'^2 + Z''^2\right)} = \frac{\cos\delta}{\omega\varepsilon_0 g\ |Z|}; \qquad \text{(SOM 4)}$$

$$\sigma' = \frac{Z'}{g\ \left(Z'^2 + Z''^2\right)} = \frac{\cos\delta}{g\ |Z|};\ \sigma'' = \frac{-Z''}{g\ \left(Z'^2 + Z''^2\right)} = \frac{-\sin\delta}{g\ |Z|}; \qquad \text{(SOM 5)}$$

where ε_0 is the permittivity of vacuum and g the geometrical factor given by current cross section A divided by contact distance d ($g = A/d$). For a series of two ideal RC elements this leads to the following expressions for the dielectric permittivity ε' and the dielectric loss ε'':

$$\varepsilon'(\omega, R_1, R_2, C_1, C_2) = \frac{C_1R_1^2 + C_1R_1^2\omega^2C_2^2R_2^2 + C_2R_2^2 + C_2R_2^2\omega^2C_1^2R_1^2}{R_1^2\omega^2C_2^2R_2^2 + 2\omega^2C_1R_1^2C_2R_2^2 + 2R_1R_2 + R_2^2\omega^2C_1^2R_1^2 + R_1^2 + R_2^2} \qquad \text{(SOM 6)}$$

$$\varepsilon''(\omega, R_1, R_2, C_1, C_2) = \frac{R_1 + R_1\omega^2C_2^2R_2^2 + R_2 + R_2\omega^2C_1^2R_1^2}{\left(R_1^2\omega^2C_2^2R_2^2 + 2\omega^2C_1R_1^2C_2R_2^2 + 2R_1R_2 + R_2^2\omega^2C_1^2R_1^2 + R_1^2 + R_2^2\right)\omega} \qquad \text{(SOM 7)}$$

In the main part of this work the curves of ε' vs temperature T and ε' vs frequency f were simulated for a series of two ideal dielectric relaxations as represented by a series of two RC elements (main text Figure 1). A step-like increase of ε' with increasing T (ε' vs T) or a step-like decrease with increasing f (ε' vs f) was demonstrated. For such simulations T independent capacitors (C_1, C_2) and Arrhenius activated resistors ($R_n = R_1$, R_2) were used (see Inset in main text Figure 1). In the SOM Figures 1a and 1b the equivalent simulations for the behavior of the dielectric loss ε'' vs T and ε'' vs f are presented.

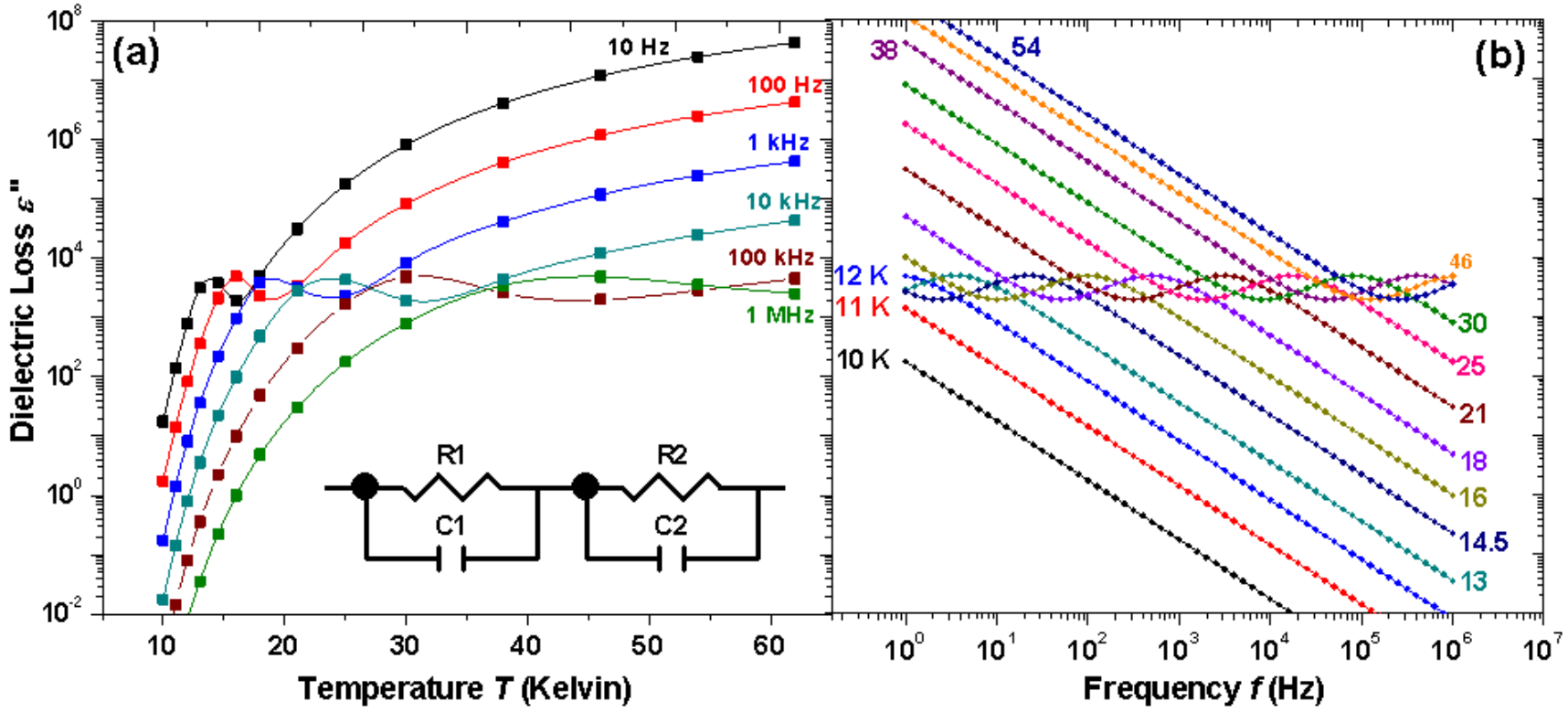

SOM Figure 1 (a) (Color online) Simulated ε" vs T data at selected frequencies (as indicated) for a series of two RC elements (see Inset). The ε" vs T curves were calculated from the analytical expression for $\varepsilon"(f, R_1, R_2, C_1, C_2)$ for a series of two RC elements, where the resistance ($R_n = R_1, R_2$) and capacitance (C_1, C_2) values were substituted according to the expressions shown in the inset of Fig. 1a in the main text. **(b)** Simulated ε" vs f data at selected temperatures as indicated. The ε" vs f curves were calculated from the analytical expression for $\varepsilon"(f, R_1, R_2, C_1, C_2)$ for a series of two RC elements.

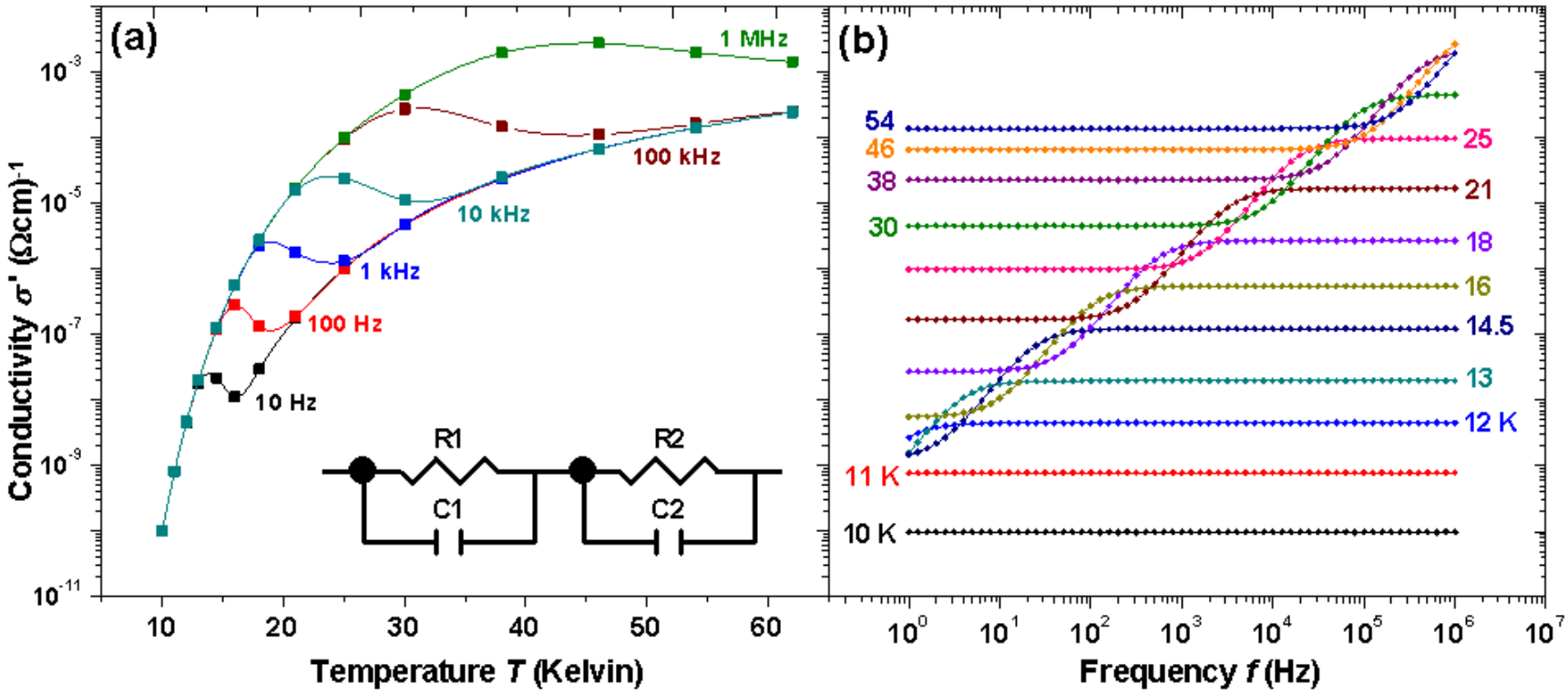

SOM Figure 2 (a) (Color online) Simulated σ' vs T data at selected frequencies (as indicated) for a series of two RC elements (see Inset). The σ' vs T curves were calculated from the analytical expression for $\sigma'(f, R_1, R_2, C_1, C_2)$ for a series of two RC elements, where the resistance ($R_n = R_1, R_2$) and capacitance (C_1, C_2) values were substituted according to the expressions shown in the inset of Fig. 1a in the main text. **(b)** Simulated σ'' vs f data at selected temperatures as indicated. The σ' vs f curves were calculated from the analytical expression for $\sigma'(f, R_1, R_2, C_1, C_2)$ for a series of two RC elements.

In SOM Figures 1a and 1b local maxima and local minima occur in both notations ε'' vs T and ε'' vs f, which are unique features of a series of two dielectric relaxations. For only one relaxation no such maxima or minima are present. The conditions for a maxima or minima in ε'' vs f can be calculated from the analytical expression for $\varepsilon''(f,R_1,R_2,C_1,C_2)$, but the resulting terms are very large. It is important to note that the local maxima and minima in SOM Figure 1 are an intrinsic feature of a series of two dielectric relaxations and should always be distinguished from a magneto-electric coupling (MEC) effect.

In the SOM Figs. 2a and 2b the behavior of the real part of the complex conductivity σ' vs T and σ' vs f is illustrated. The σ' vs T curves show local minima and maxima at identical temperatures as the ε'' vs T curves (SOM Figure 1a). This congruence is a consequence of the similarity of σ' and ε'', as is demonstrated in equations (SOM 4) and (SOM 5).

In the σ' vs f curves (SOM Figure 2b) two plateaus can be seen at sufficiently high temperatures, which is reminiscent of the two plateaus shown in Figures 1a and 1b in the main text. The drop occurs at different f here though and the two plateaus now represent the different resistance values of R1 and R2, whereas the two plateaus in Figure 1 (main text) represent the different capacitance values of C1 and C2.

It should be noted that it is unlikely that the curves of σ' vs T and σ' vs f for a series of two ideal relaxations presented in the SOM Figure 2 appear in the same or in a similar fashion for real experimental data. The σ' vs T and σ' vs f curves are highly susceptible to potential non-ideality of the respective dielectric relaxations and the shape of the curves changes drastically for non-ideal relaxations. This is demonstrated below for experimental data from $BiMnO_3$ (BMO) and $BiFeO_3$ (BFO) thin films (SOM Part VII).

II. BMO and BFO thin film deposition

Thin films of BFO (100 nm) and BMO (50 nm) were grown on (001)-oriented 0.5% Nb-doped STO substrates from 10% Bi-rich targets using pulsed laser deposition (1.8 J/cm^2 laser fluence and 5 Hz repetition rate) following the procedures reported previously.[3,4] The BMO phase could be stabilized in a narrow window of deposition conditions at 650ºC substrate temperature under 0.1 mbar of oxygen partial pressure. For BFO 675ºC and 0.1 mbar proved to be the optimum conditions. After deposition films were cooled to room temperature under oxygen atmosphere.

III. X-ray diffraction of thin films

X-ray diffraction (XRD) on BMO and BFO films was carried out using a PANalytical Pro MRD 4-circle diffractometer using Cu K_α radiation. The BMO and BFO film θ-2θ XRD pattern (SOM Figure 1) reveal the absence of parasitic phases. The (0k0) BMO and (00•) BFO pseudo-cubic reflections correspond to out-of-plane lattice parameters of ≈ 3.99 Å (BMO) and ≈ 4.04 Å (BFO). In BMO the ***a*** and ***c*** bulk lattice parameters (***a*** ≈ ***c*** ≈ 3.935 Å) exhibit a compressive mismatch of -0.77% with the STO cubic lattice parameter ($\boldsymbol{a}_{STO}$ = 3.905 Å), whereas the ***b*** lattice parameter (3.989 Å) exhibits a larger mismatch and a potential compressive strain of -2.15%. It is hence commonly accepted that the ***b***-axis in BMO is the one which stands out-of-plane.

Bulk BFO has previously been indexed as *R3c* rhombohedral crystal symmetry with ***a*** = ***b*** = ***c*** = 5.634 Å,[5] whereas in the pseudo-cubic notation ***a*** = ***b*** = ***c*** = 3.965 Å has been reported.[6] By clamping the pseudo-cubic unit cell to the substrate by epitaxial constraint a compressive in-plane strain of -1.54% occurs in the BFO film, when coherently grown. The out-of-plane orientation in BFO films can be ascribed to any of the pseudo-cubic crystallographic axes, but commonly the ***c*** axis is regarded as out-of-plane.[7]

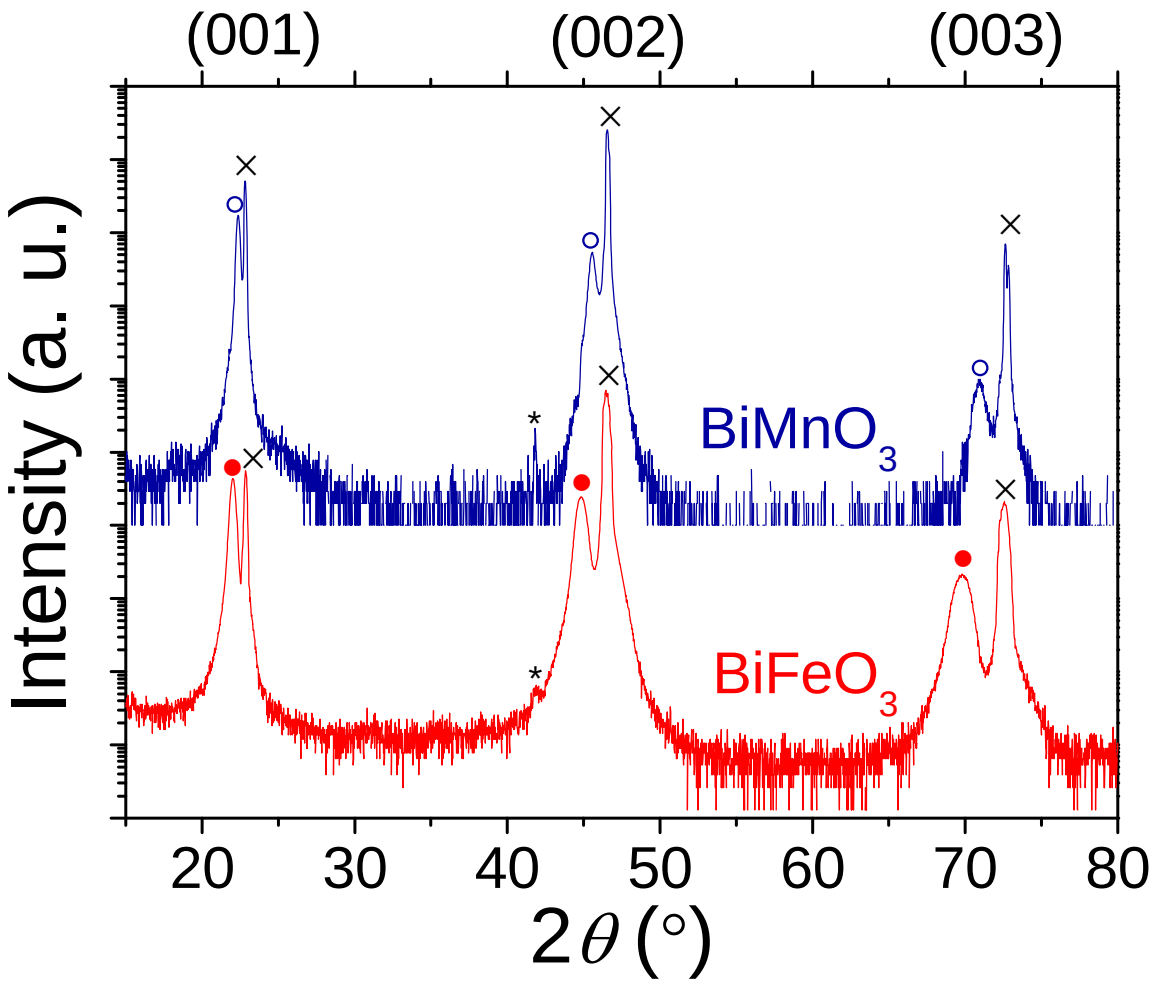

SOM Figure 3: XRD symmetric θ-2θ diffractograms of the BMO (top) and BFO films (bottom). The (001), (002) and (003) substrate peaks are indicated by crosses (x), whereas (0k0) and (00ℓ) pseudocubic reflections of BMO and BFO are labeled with empty and filled circles (○,●), respectively. The asterisks (*) indicate the $SrTiO_3$ (002) peak caused by Cu K_β radiation.

BMO and BFO films were grown in a single cube-on-cube fashion, as inferred from XRD θ-2θ diffractograms (SOM Figure 3) and phi-scans (not shown). The former proved single orientation of the films in the out-of-plane direction, whereas the latter showed in-plane single orientation and full alignment with STO. According to the reciprocal space maps around the STO (204) reflection (insets in SOM Figures 4a and 4b), $q_{||}$ of BMO and BFO appear to be identical to that

of the substrate and both type of films are found to exhibit coherent growth on Nb-STO substrates. A previous report on BFO films grown on (001) STO mentioned a monoclinic distortion for films thicker than 20 nm.[8] Due to instrumentally limited peak broadening here it was not possible to discern between the small monoclinic distortion and the tetragonal unit cell. The thickness of the films was determined by means of X-ray reflectometry.

IV. Atomic Force Microscopy (AFM)

The structure and surface morphology of BMO and BFO films were characterized by Atomic Force Microscopy (AFM, Agilent 5420). The (001) faceted BMO and BFO crystallites can be seen in the AFM topography images (SOM Figures 4a and 4b respectively).

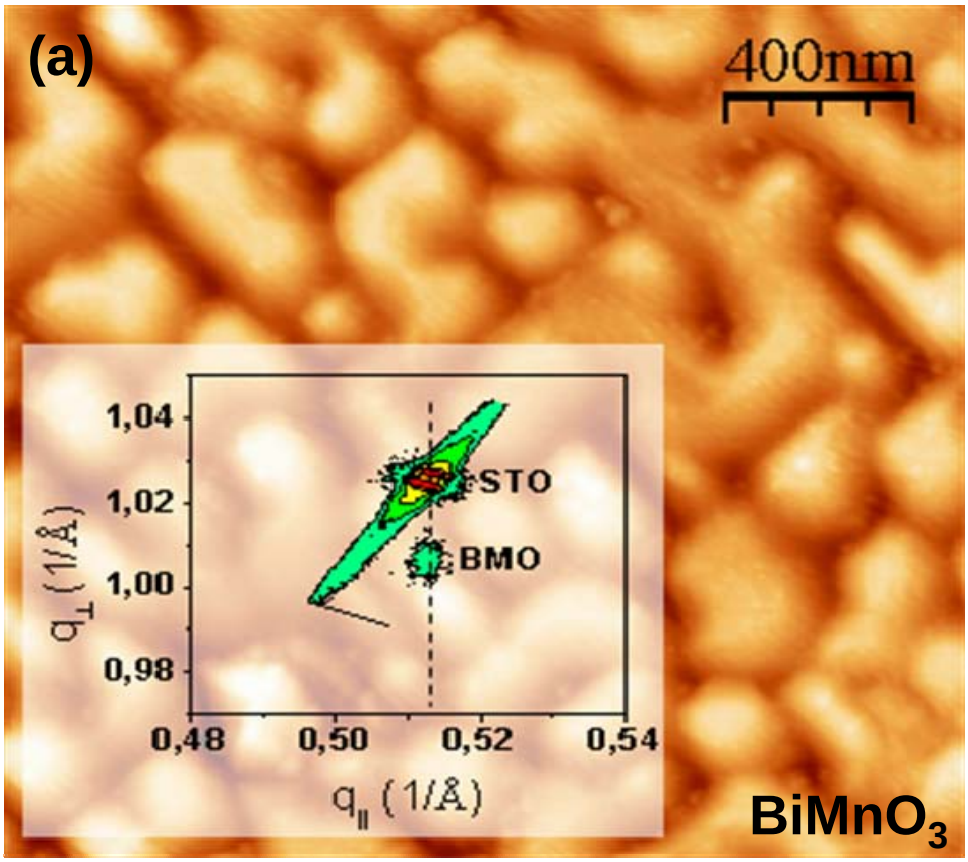

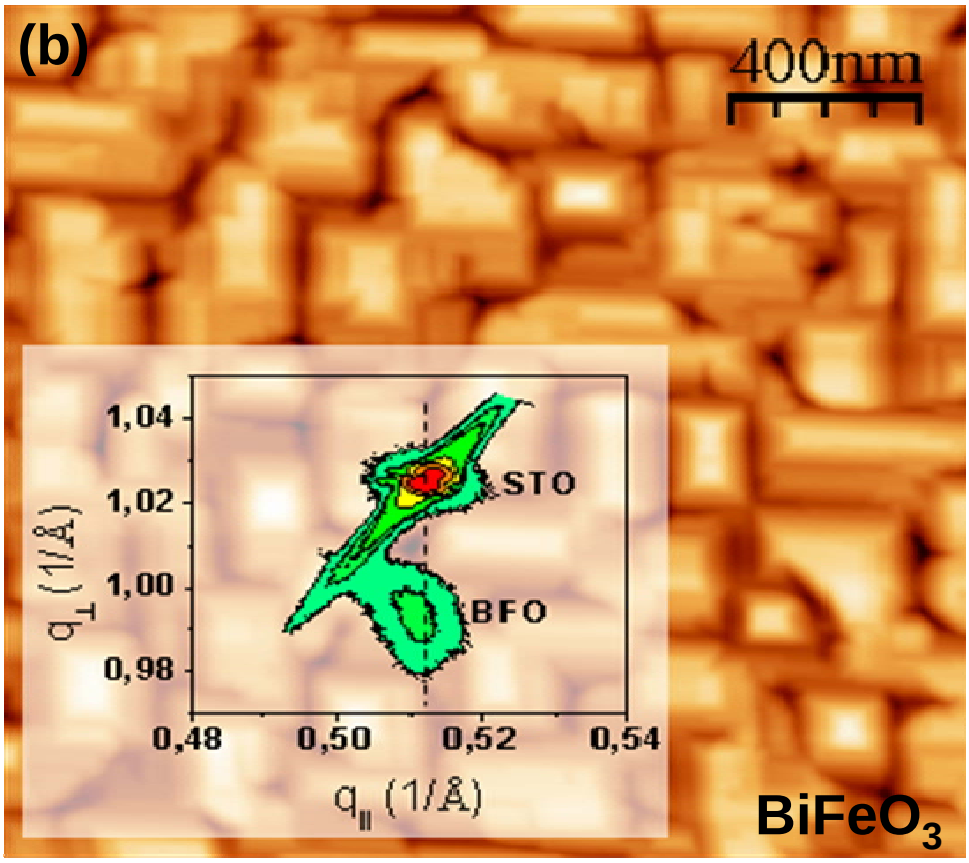

SOM Figure 4: AFM topography images (2x2 μm^2) of **(a)** $BiMnO_3$, and **(b)** $BiFeO_3$. **Insets:** XRD reciprocal space maps around the (204) reflection of $SrTiO_3$.

The (001) facets were identified from the distribution of angles on the AFM topography data. The total alignment of these objects evidences that the films are single crystal domain and according to the structural characterization they follow the crystallographic directions of the STO substrate. The surfaces of the films have been checked to be continuous with complete coalescence and a RMS roughness of around 5% of the nominal film thickness.

V. Piezo-force microscopy

Room temperature piezo-response force microscopy (PFM) was performed on BFO films (Nanomagnetics Inst.). Images were acquired using Si tips with PtIr coating at an AC voltage of 0.5 Vrms and a frequency of 50 kHz. Ferroelectric domains were written by applying a DC voltage between the conducting microscope tip and the Nb-STO bottom electrode. In the set-up used here voltages were applied to the sample while the tip was grounded. In BFO, well-defined poled areas were patterned by applying a DC voltage between tip and substrate, and subsequently checked by piezo-response force microscopy (PFM). Simultaneous topographic and out-of-plane PFM phase and amplitude images (SOM Figures 5a, 5b and 5c) were recorded.

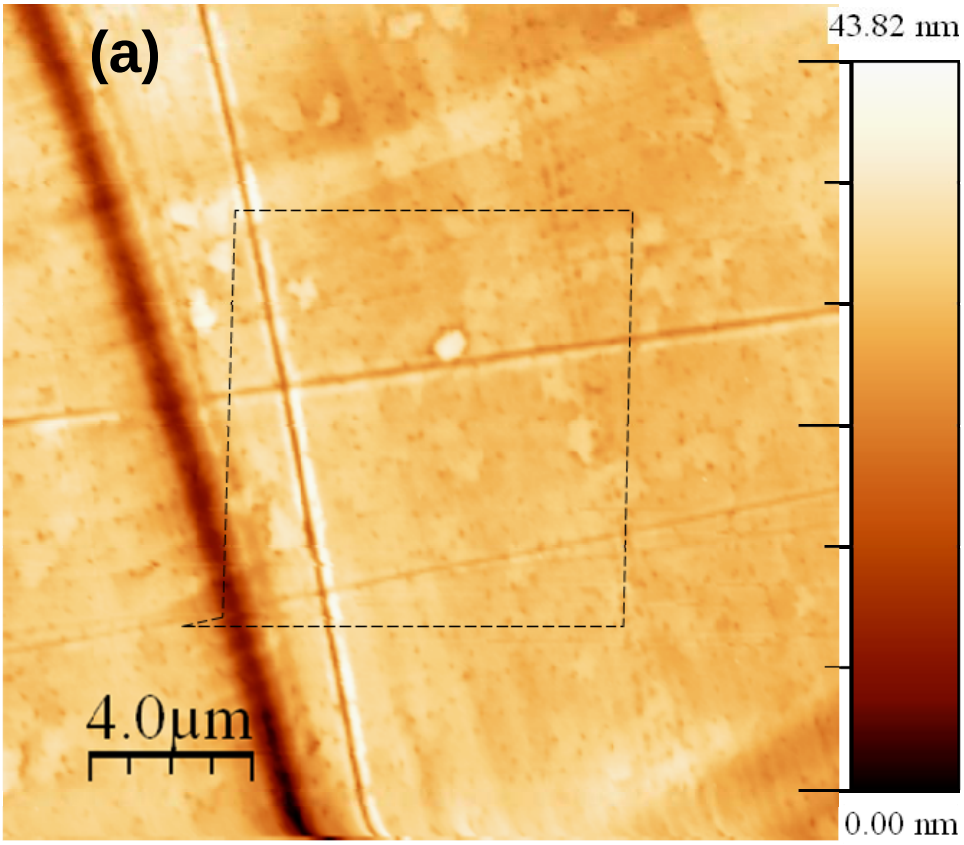

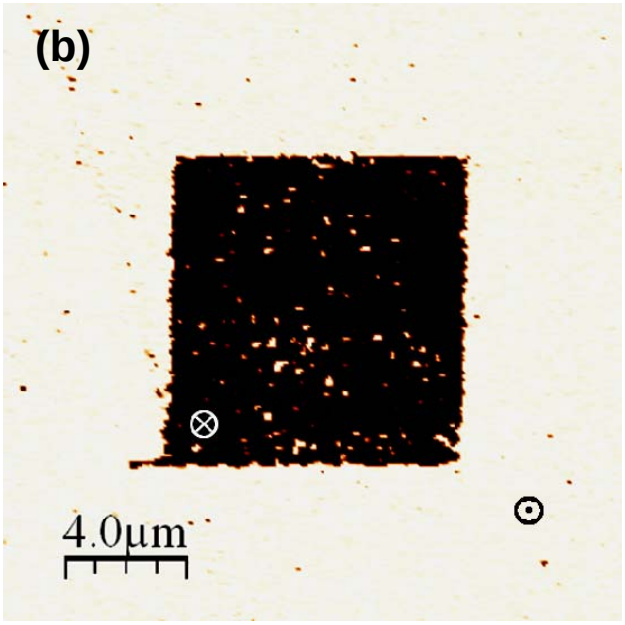

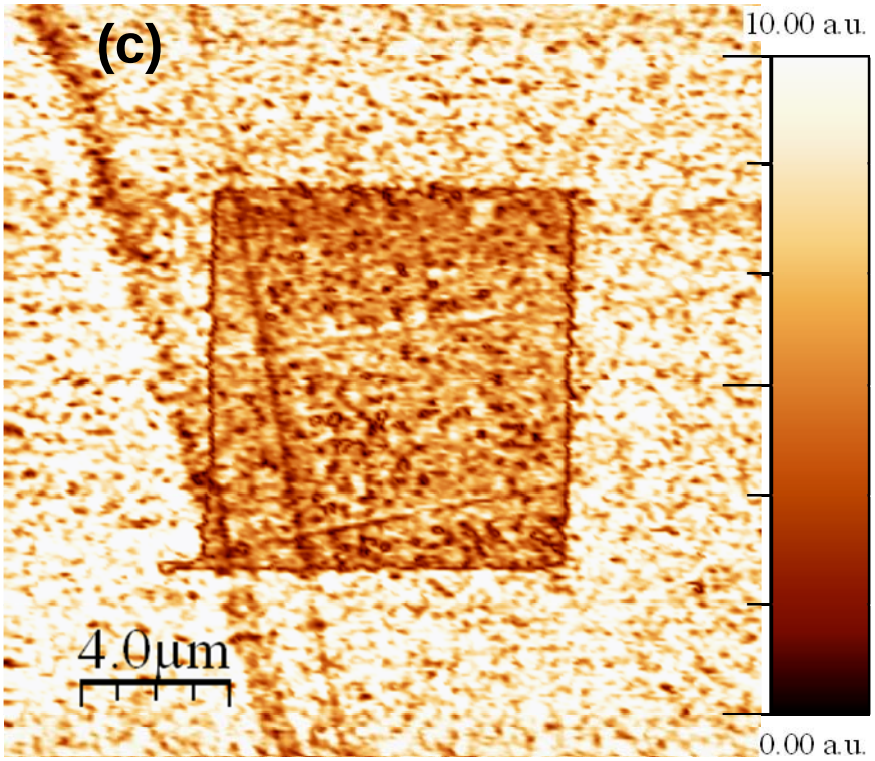

SOM Figure 5: (a) Surface topography, **(b)** out-of-plane PFM phase, and **(c)** out-of-plane PFM amplitude images of $BiFeO_3$ (20x20 μm^2) thin film. The marked area in **(a)** was previously scanned by applying a DC voltage (-5V) between tip and substrate.

The topographic image in SOM Figure 5a shows that switching the polarization within the marked area does not damage the BFO film surface. The phase image in SOM Figure 5b presents a 180º contrast between the poled area and the surrounding film, pointing to the switching of the perpendicular component of the polarization, with a corresponding minimum in the amplitude image at the domain wall (SOM Figure 5c). Polarization can be switched back and forth by reversing the polarity of the applied voltage, confirming that the BFO film was ferroelectric at room temperature.

PFM on BMO films did not succeed due to low film resistance at room temperature.

VI. Magnetic film characterization

The magnetic properties of BMO and BFO films were determined using SQUID magnetometry (Quantum Design MPMS XL) with magnetic field applied in the film in-plane direction. The ferromagnetic moment in BMO thin films is clearly observed in the hysteretic magnetization (M) vs applied magnetic field (H) curve recorded at 5 K (SOM Figure 6). A saturated BMO moment of $M_{sat.} \approx 2.5\ \mu_B$/Mn was found, which is smaller than the bulk value (3.6 μ_B/Mn) but close to the thin film value reported previously (2.2 μ_B/Mn).[4] A BMO coercive field $H_{coerc.}$ of ≈ 425 Oe (upper inset of SOM Figure 6) was found. The temperature dependence of M under 1 kOe applied H and the differentiated inverse of the magnetic susceptibility ($1/\chi = 1/M$) (lower inset of SOM Figure 6) allowed determining the ferromagnetic Curie temperature $T_C \approx 100$ K, in close agreement to the bulk value.[9-11]

The BFO film showed signs of anitferromagnetism with a weak ferromagnetic moment up to room temperature (SOM Figure 7). The $M_{sat.} \approx 0.05\ \mu_B$/Fe registered at 5 K agrees with previous

reports.[3, 12-14] The appearance of a small ferromagnetic component in epitaxial BFO thin films may be ascribed to spin canting due to lattice or FE domain wall strain or oxygen vacancies.[14]

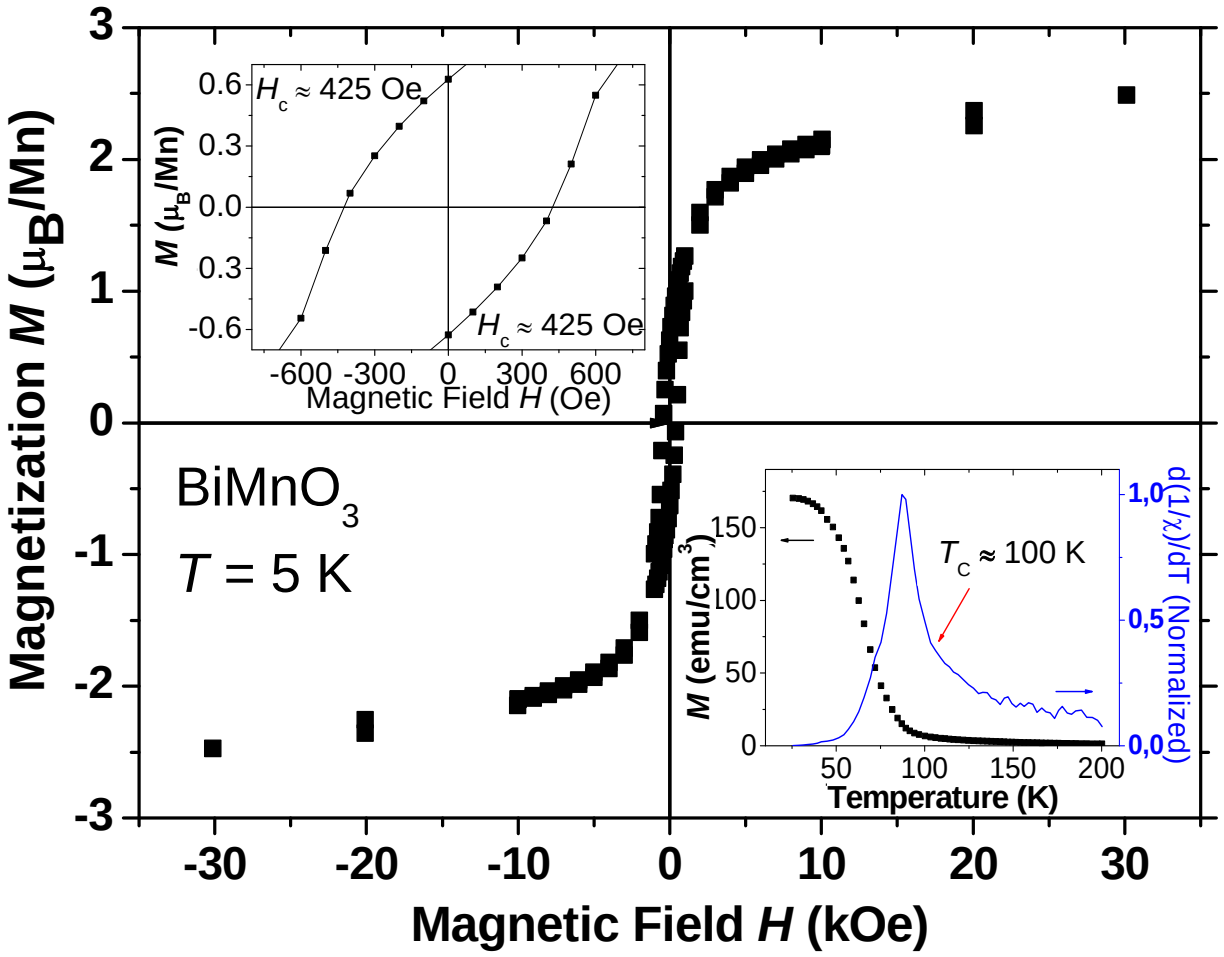

SOM Figure 6: *H* dependence of magnetization *M* for BMO thin films at 5 K. **Upper inset:** zoom of the low-field region. **Lower inset:** *T* dependence of *M* under field-cooled (FC) conditions using an external in-plane field of *H* = 1 kOe (left axis) and derivative of the inverse susceptibility (right axis).

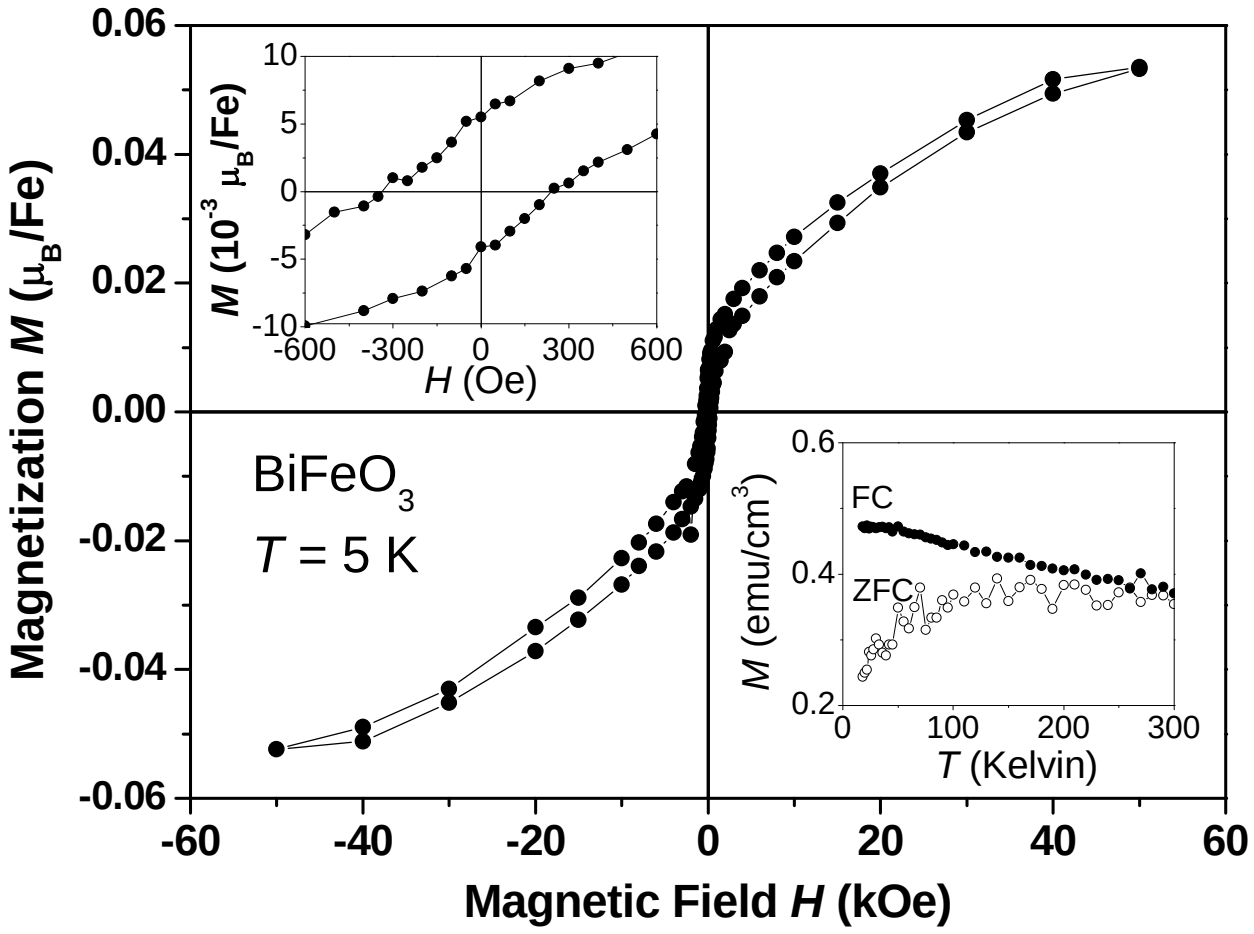

SOM Figure 7: *H* dependence of *M* for BFO thin films at 5 K. **Upper inset:** zoom of the low-field region. **Lower inset:** Zero-field cooled (ZFC) and field cooled (FC) *M* vs *T* curves using an external in-plane magnetic field of 100 Oe.

VII. Alternative representations of dielectric spectroscopy data

The dielectric loss ε" curves collected from a 50 nm BMO film without applied magnetic field are plotted in the SOM Figure 8a in terms of ε" vs f.

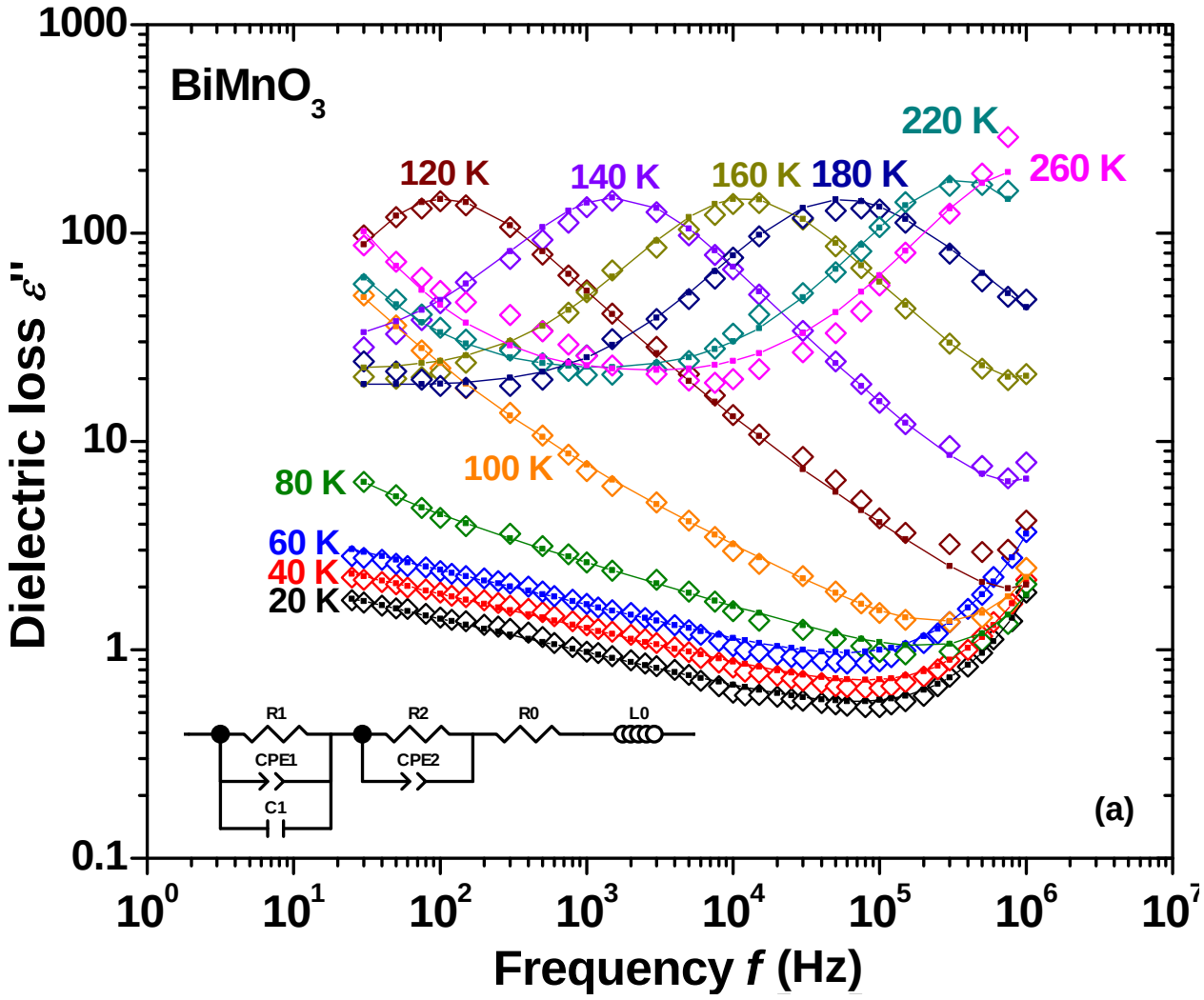

SOM Figure 8 (a) Dielectric loss ε" vs f for 50 nm BMO thin film at various selected temperatures as indicated. Open symbols (◊) represent experimental data, full squares (■) and solid lines represent fits to the data using the equivalent circuit depicted below the curves. The occurrence of local maxima and minima is consistent with the expected behavior of a series of two dielectric relaxations. No MEC effect is required to explain such behavior.

At low T the loss is relatively low, whereas at higher T the losses increase and the local maxima and minima occur as expected for a series of two dielectric relaxations (see SOM Figure 1b). The local maxima are much broader though as expected for ideal relaxations presented in the SOM Figure 1b, which indicates a certain degree of non-ideality. Such non-ideality has been accounted for in the equivalent circuit by the use of a Constant-Phase Element (CPE). The small MEC effect in BMO reported in the main text can not account for the maxima observed at 120 K and above in SOM Figure 8a. Such maxima are fully consistent with a series of two relaxations, which is confirmed by the good agreement between data and the model based on a series of two RC elements. The sharp upturn of ε" at high f (mainly at low T) is due to L0.

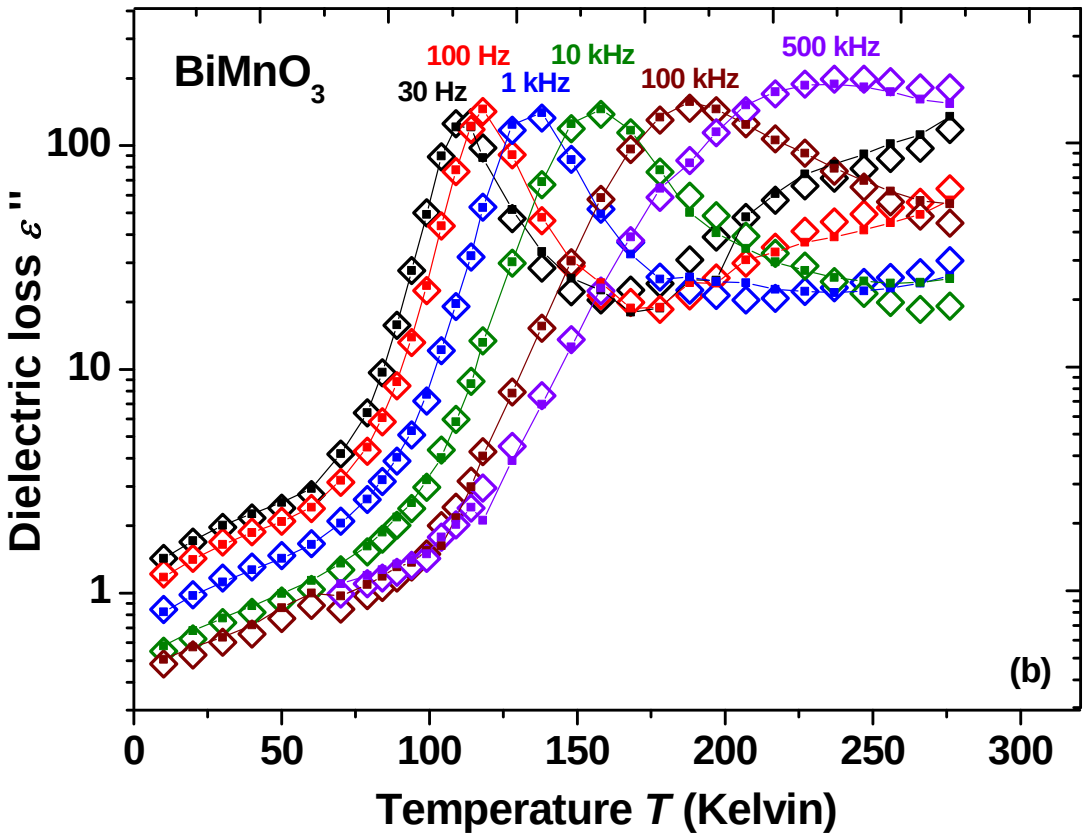

SOM Figure 8 (b) Identical data and fits as in SOM Figure 8a, transposed into the ε" vs T notation at selected frequencies as indicated.

The T dependent notation of ε" vs T is shown in the SOM Figure 8b. Local maxima and minima occur as expected for a series of two dielectric relaxations (see SOM Figure 1a), where the minimum is fully developed only up to 1 kHz. Such maxima and minima may again not be mistaken for an MEC effect.

The T and f dependent BMO thin film dielectric data was also converted into the conductivity notation σ' vs f and σ' vs T, as shown in SOM Figures 9a and 9b respectively.

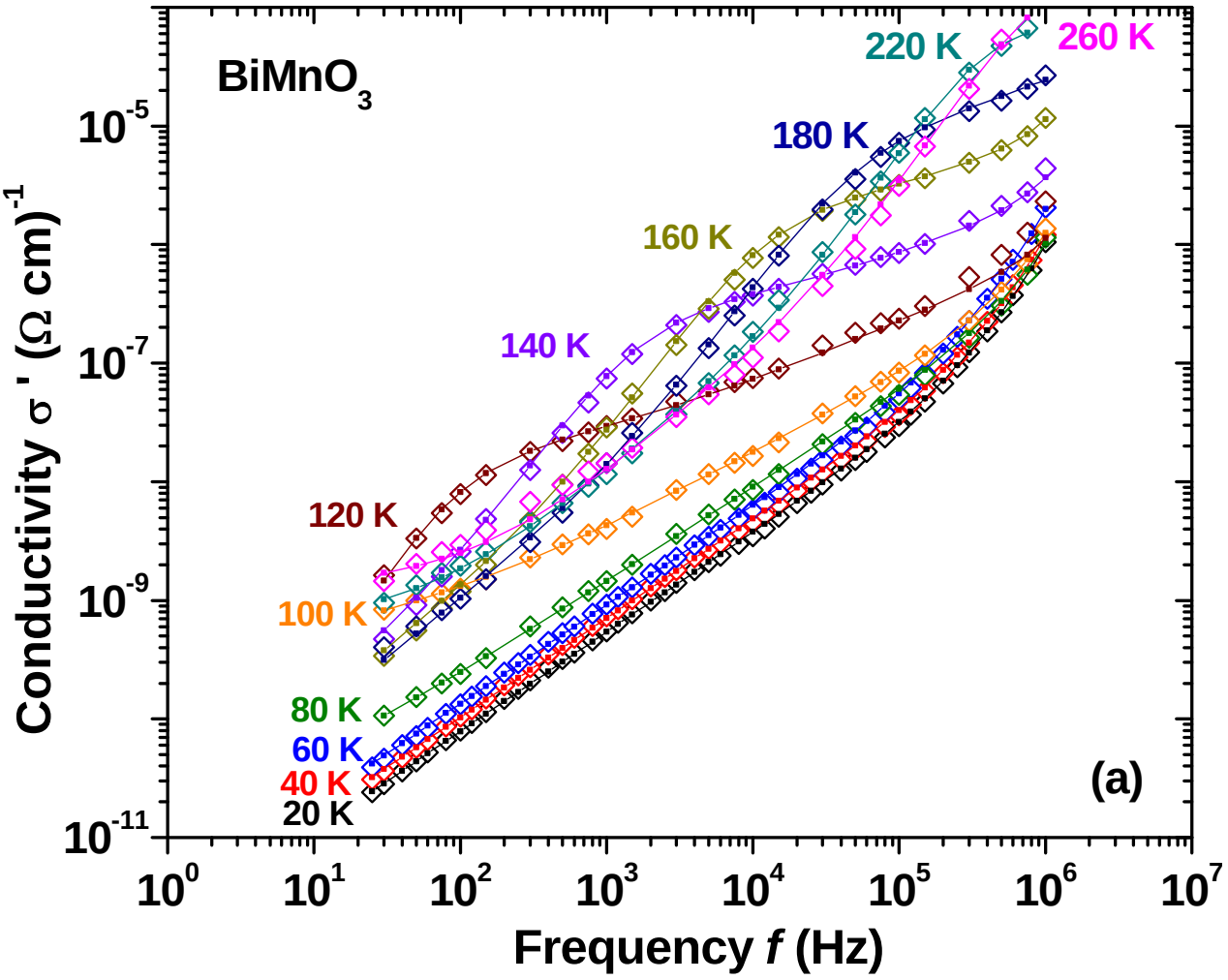

SOM Figure 9 (a) Identical data and fits as in SOM Figure 8, transposed into the σ' vs f notation at selected temperatures as indicated.

The σ' vs f data contains clear signs of the non-ideality of the intrinsic BMO relaxation, especially at low temperatures (20 K – 80 K). In this regime an f independent σ' plateau is expected (see SOM Figure 2b). Instead, significant dispersion of σ' with f is indicated, which can be associated with a Jonscher type dielectric response.[15] The additional upturn of σ' at high f is due to the inductor L0. Two σ' plateaus as expected for a series of two dielectric relaxation are fully visible only at 220 K and 260 K. The non-ideality of the intrinsic BMO relaxation is also manifested in plots of σ' vs T shown below (SOM Figure 9b), which differ significantly from the behavior of a series of two ideal dielectric relaxations as depicted in the SOM Figure 2a.

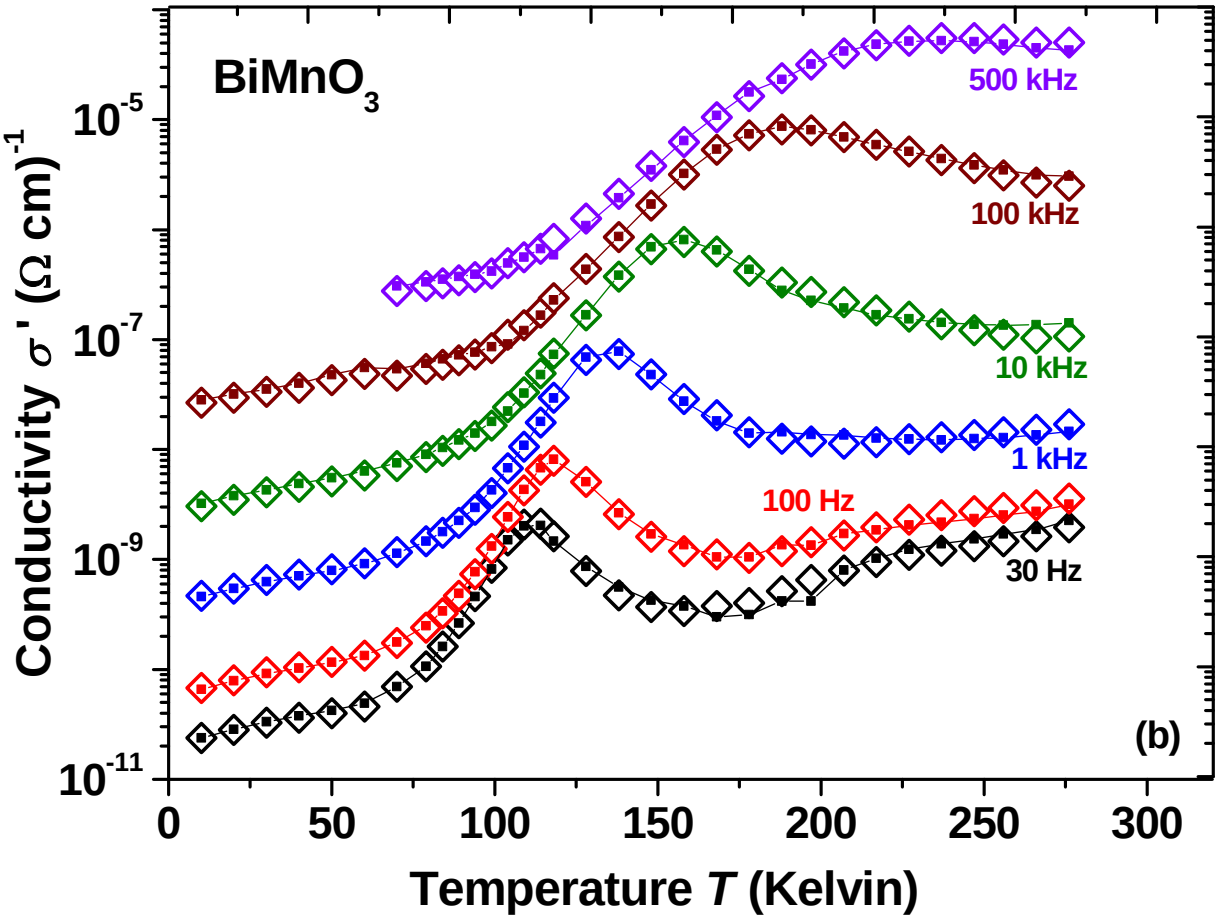

SOM Figure 9 (b) Identical data and fits as in SOM Figure 9a, transposed into the σ' vs T notation at selected frequencies as indicated.

It should be noted that the clear peak features near 100 K in SOM Figure 9b are fully consistent with the presence of two dielectric relaxations and may not be interpreted as an MEC effect at the magnetic transition T_C. This is particularly obvious at higher f, where the peak slightly shifts to higher T. A potential shift of T_C to higher T with increasing f is not reasonable. In fact, the equivalent circuit model takes full account of the peak structure although the model is not influenced by the MEC effect in this instance.

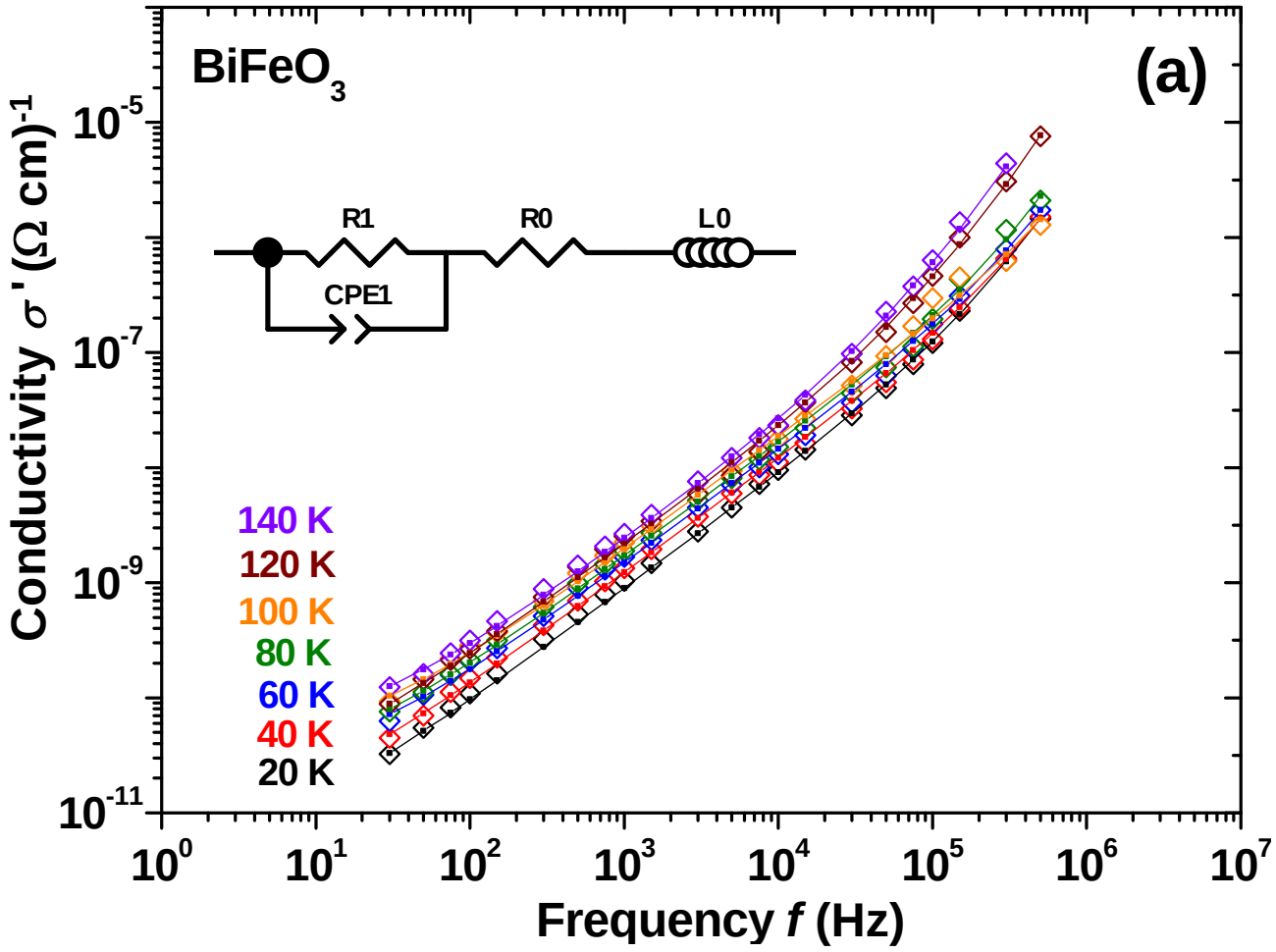

SOM Figure 10 (a) Conductivity σ' vs f for 100 nm BFO thin film at various selected temperatures as indicated. Open symbols (◊) represent experimental data, full squares (■) and solid lines represent fits to the data using the equivalent circuit depicted above the curves.

The dielectric permittivity ε' and dielectric loss ε'' for BFO have been presented in the f dependent notation in Figure 3a in the main text, whereas the ε' vs T curves are shown in the main text in Figure 3b. The ε'' vs T curves do not provide any significant new insight and their trends are obvious from the Figure 3a Inset in the main text. Therefore, such curves are not shown here and the T and f dependent BFO thin film dielectric data is presented here only in the conductivity σ' notation. In the T range investigated only the intrinsic BFO thin film relaxation was detected and, accordingly, σ' shows straight forward T and f dependences as demonstrated in the SOM Figures 10a and 10b.

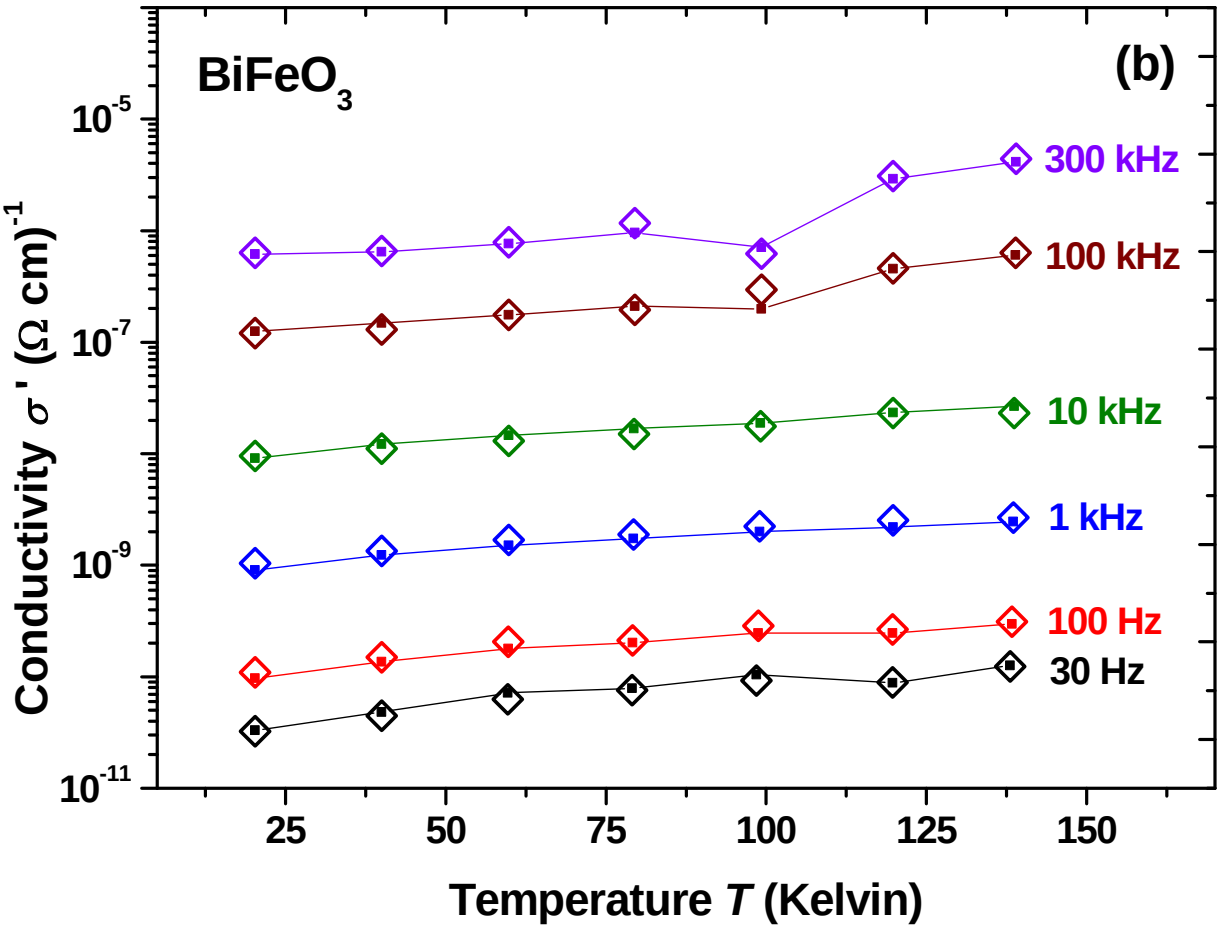

SOM Figure 10 (b) Identical data and fits as in SOM Fig. 10, transposed into the σ' vs T notation at selected temperatures as indicated.

SOM Figure 10 (b) shows a weak T dependence of σ', which is untypical for the expected thermally activated charge transport in insulating $BiFeO_3$ thin film. A possible explanation for such behavior could be a conduction mechanism based on electron transport by quantum mechanical tunneling between localized impurity states, which is indeed expected to be T independent.[16] Another more favorable explanation may be the strong f dependence of σ' as demonstrated in the SOM Figure 10a. Such strong f dependence of σ' points towards a Jonscher type dielectric response, where in the high f regime approximately T independent dispersion of σ' with f is expected.[15]

Supplementary Online Materials References:

[1] E. Barsukov, J.R. Macdonald, *Impedance Spectroscopy: Theory, Experiment and Applications*, John Wiley & Sons Inc. (Holboken), 2005

[2] R. Schmidt, Impedance Spectroscopy of Electroceramics, in *Ceramic Materials Research Trends*, Novascience Publishers (Hauppauge), 2007

[3] W. Eerenstein, F. D. Morrison, J. Dho, et al., Science **307**, 1203a (2005).

[4] W. Eerenstein, F. D. Morrison, J. F. Scott, et al., Appl. Phys. Lett. **87**, 101906 (2005).

[5] J. Wang, J. Neaton, H. Zheng, et al., Science **299**, 1719 (2003).

[6] F. Kubel and H. Schmid, Acta Cryst. B **46**, 698 (1990).

[7] J. F. Ihlefeld, A. Kumar, V. Gopalan, et al., Appl. Phys. Lett. **91**, 071922 (2007).

[8] C. J. M. Daumont, S. Farokhipoor, A. Ferri, et al., Phys. Rev. B **81**, 144115 (2010).

[9] H. Chiba, T. Atou, and Y. Syono, Journal of Solid State Chem. **132**, 139 (1997).

[10] F. Sugawara, S. Iiida, Y. Syono, et al., J. Phys. Soc. J. **25**, 1553 (1968).

[11] H. Faqir, H. Chiba, M. Kikuchi, et al., J. Solid State Chem. **142**, 113 (1999).

[12] H. Béa, M. Bibes, A. Barthélémy, et al., Appl. Phys. Lett. **87**, 072508 (2005).

[13] M. Bai, J. L. Wang, M. Wuttig, et al., Appl. Phys. Lett. **86**, 032511 (2005).

[14] V. G. Prokhorov, G. G. Kaminsky, J. M. Kim, et al., Low Temp. Phys. **37**, 129 (2011).

[15] A.K. Jonscher, Dielectric Relaxation in Solids, Chelsea Dielectrics (London), 1983

[16] U. Weiss, *Quantum Dissipative Systems*, Series in Modern Condensed Matter Physics Vol. 13, World Scientific (Singapore), 2001